

# Theoretical study of the excited states of NeH and of their non-adiabatic couplings: a preliminary for the modeling of the dissociative recombination of NeH<sup>+</sup>

R. Hassaine<sup>1,\*</sup>, D. Talbi<sup>2,†</sup>, R. P. Brady<sup>3,‡</sup>, J. Zs. Mezei<sup>1,4,§</sup>, J. Tennyson<sup>1,3,¶</sup> and Ioan F. Schneider<sup>1,5,\*\*</sup>

<sup>1</sup>LOMC CNRS-UMR6294, Université le Havre Normandie, F-76058 Le Havre, France

<sup>2</sup>LUPM CNRS-UMR5299, Université de Montpellier, F-34095 Montpellier, France

<sup>3</sup>Dept. of Physics and Astronomy, University College London, WC1E 6BT London, UK

<sup>4</sup>HUN-REN Institute for Nuclear Research (ATOMKI), H-4001 Debrecen, Hungary and

<sup>5</sup>LAC-UMR9188, CNRS Université Paris-Saclay, F-91405 Orsay, France

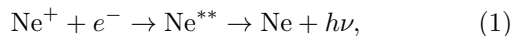
(Dated: January 31, 2025)

Potential energy curves and matrix elements of radial non-adiabatic couplings of <sup>2</sup>Σ<sup>+</sup> and <sup>2</sup>Π states of the NeH molecule are calculated using the electronic structure package MOLPRO, in view of the study of the reactive collisions between low-energy electrons and NeH<sup>+</sup>.

PACS numbers:

## I. INTRODUCTION

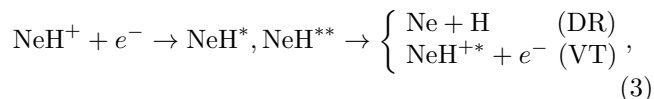
Neon is envisaged as a coolant in the divertor of the International Thermonuclear Experimental Reactor (ITER) [1–4], since it can absorb energy via its excitation and ionization through reactions with rapid electrons. Dielectronic recombination of the formed ions, followed by electronic relaxation process:



allows safe dissipation of heat along the walls through radiation. On and near the surface of the reactor, collisions between neon atoms with vibrationally excited H<sub>2</sub><sup>+</sup> can produce NeH<sup>+</sup>:



the reaction for ground state ions being endothermic by 0.54 eV.[3] The presence of NeH<sup>+</sup> in the edge plasma implies the need for quantifying the reactivity of this ion. This can be achieved from the calculation of the cross sections and rate coefficients which characterize the efficiency of collisions between NeH<sup>+</sup> and other species present in the plasma. Among them, the collisions with electrons, resulting in dissociative recombination (DR)[4] and vibrational transitions (VT):



are particularly important.

Cross sections for the DR of NeH<sup>+</sup> were already measured at the storage ASTRID ring two decades ago [3]. Theoretical evaluations of the cross sections have also been performed for collision energies ranging between 5

and 22 eV [4], and they agree with the experimental ones between 6 and 10 eV. So far, theoretical results are not available for the physically important electron collision energies below 5 eV, where experiment [3] measures significant cross sections of about 10<sup>-18</sup> cm<sup>2</sup>.

The low energy DR of the hydride cations relying on the elements preceding and following neon in the periodic tables - helium and argon respectively - is well understood and quantified. Both present in the edge plasma, they were object of detailed investigations related mainly on their abundances in the interstellar media.

HeH<sup>+</sup>, one of the oldest molecule in the Universe, was only recently observed in the nebula NGC 7027 [5]. It is the simplest molecular prototype that recombines with electrons exclusively through the indirect pathway, proceeding via electron capture into Rydberg states, without having a diabatic dissociative neutral state that crosses the cation [6, 7]. The initial state-selective measurements performed on the Cryogenic Storage Ring [8] have shown a dramatic decrease of the DR rate coefficients at very low collision energies, that can cause higher abundances in cold interstellar environments. The most recent calculations of Ćurik et al [9, 10] using energy-dependent rovibrational frame transformation combined with multichannel quantum defect theory have confirmed the experimental observations.

As for ArH<sup>+</sup>, it was detected more than one decade ago in the Crab Nebula [11]. Prior to its discovery, Mitchell et al [12], working in the ASTRID storage ring, had estimated the anisotropic rate coefficient below 2 eV lower than 10<sup>-9</sup> cm<sup>3</sup>s<sup>-1</sup>. Some of us addressed the molecular structure of ArH [13] and found that the asymptotic limit of the lowest diabatic electronic state of this molecule is 1.822 eV above the ground vibrational level, which implies - if restricted exclusively to Rydberg-valence coupling - no recombination below this energy and, consequently, a negligible rate coefficient [14]. However, Kalosi et al [15] measured low but non-negligible DR rates into the ground state of ArH, claiming the mechanism of non-adiabatic coupling between the ionization continuum and the ground electronic state. This scenario is supported by theoretical considerations in the same study, as well as computations in progress by Larson and Orel [15].

Unlike HeH<sup>+</sup> [5] and ArH<sup>+</sup> [11], NeH<sup>+</sup> remains undetected in these media. Recent work by Sil et al[16]

\*riyad.hassaine@univ-lehavre.fr

†dahbia.talbi@umontpellier.fr

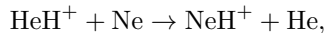
‡ryan.brady.17@ucl.ac.uk

§mezei.zsolt@atomki.hu

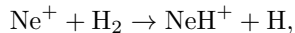
¶j.tennyson@ucl.ac.uk

\*\*ioan.schneider@univ-lehavre.fr

suggests that  $\text{NeH}^+$  could be formed in nova ejecta via the reaction:



with a rate coefficient of approximately  $10^{-9} \text{ cm}^3 \text{ s}^{-1}$ . This pathway appears more likely than the alternative reaction proposed by Theis et al[17]:



which is considered unfavorable. The formation of  $\text{NeH}^+$  is expected to be heavily dependent on the abundance of  $\text{HeH}^+$ , which is more prevalent due to the significant presence of helium and atomic hydrogen in the environment. However,  $\text{NeH}^+$  production is constrained by the comparatively low cosmological abundance of neon[18] and the underabundance of molecular hydrogen. Another potential explanation for the non-detection of  $\text{NeH}^+$  may lie in its dissociative recombination behavior. A high dissociative recombination rate coefficient at interstellar medium relevant temperatures could significantly reduce its steady-state concentration, making detection more challenging.

Below 5 eV, the lack of theoretical data for the cross sections can be initially addressed by producing the *ab initio* adiabatic potential energy curves (PECs) of  $\text{NeH}$  corresponding to the bound Rydberg states energetically open for dissociation (below  $v_i^+ = 0$  of the ion's ground state), similarly to Refs. [19–23], and non-adiabatic couplings responsible for the transitions among the different Born-Oppenheimer adiabatic states. Here we consider both the relevant  $\text{NeH}$  PECs and compute the matrix elements which give the radial non-adiabatic couplings (NACs) between all the explored states of the neutral. In the current study, we focus on these two aspects, while the dynamical calculations will be considered in a further work, relying on the current molecular structure data results.

The organisation of the paper is as follows: In section II, the computational steps are presented. Section III contains the results - PECs, spectroscopic data, NACs - and we provide the concluding remarks in section IV.

## II. COMPUTATIONAL DETAILS

The potential energy curve calculations for  $\text{NeH}$  and  $\text{NeH}^+$  in its ground state were carried out using the MOLPRO quantum chemistry program suite [24] at the MCSCF-MRCI level of theory with a complete active space (CAS) of 8,3,3,0 orbitals in the  $C_{2v}$  point-group symmetry. It corresponds to the complete valence active space extended to include the  $n = 2$  and  $n = 3$  orbitals of hydrogen. We started with the augmented correlation-consistent polarized valence triple zeta (aug-cc-pVTZ) basis sets implemented in MOLPRO, and we have extended the hydrogenic part of the basis by two  $s$ , three  $p$ , and one  $d$  diffuse orbitals (AO) with exponents from Ref. [21], which are given in table I.

In this way, the chosen basis set provides a more accurate description of the states correlating to the  $n = 2$  and  $n = 3$  hydrogen dissociation limits.

TABLE I: H atom Rydberg basis set.

Type	Exponent	Coefficient
$s$	0.006685	1.0
$s$	0.002670	1.0
$p$	0.024684	1.0
$p$	0.007169	1.0
$p$	0.002867	1.0
$d$	0.003600	1.0

For the neutral molecule, the MCSCF wave functions were optimized by state-averaging the five lowest  $^2\Sigma^+$  states (5  $A_1$  states in the  $C_{2v}$  symmetry of the calculation) and the two lowest  $^2\Pi$  states ( $^2B_2/^2B_1$  states in the  $C_{2v}$  symmetry of the calculation). To summarize, the ground state of  $\text{NeH}^+$ ,  $X \ ^1\Sigma^+$ , and the lowest 7 states of  $\text{NeH}$ , respectively  $X \ ^2\Sigma^+$ ,  $A \ ^2\Sigma^+$ ,  $B \ ^2\Pi$ ,  $C \ ^2\Sigma^+$ ,  $4 \ ^2\Sigma^+$ ,  $2 \ ^2\Pi$ , and  $5 \ ^2\Sigma^+$  have been calculated.

The NACs between states of the neutral were calculated using the following expressions [7, 25]:

$$A_{ij}(R) = \left\langle \psi_i^\Gamma(\{\vec{r}\}, R) \left| \frac{\partial}{\partial R} \right| \psi_j^\Gamma(\{\vec{r}\}, R) \right\rangle_{\{\vec{r}\}} \quad (4)$$

$$B_{ij}(R) = \left\langle \psi_i^\Gamma(\{\vec{r}\}, R) \left| \frac{\partial^2}{\partial R^2} \right| \psi_j^\Gamma(\{\vec{r}\}, R) \right\rangle_{\{\vec{r}\}} = \frac{\partial A_{ij}(R)}{\partial R} - A_{ij}^2(R) \quad (5)$$

Here  $\Gamma$  stands for the symmetry of the molecular state,  $i$  and  $j$  denote different electronic states belonging to the same symmetry, and we focus exclusively on couplings that satisfy  $i < j$ .  $R$  is the internuclear distance,  $\{\vec{r}\}$  denotes the complete set of electronic coordinates linked

to the electrons of the neutral. In order to calculate the NACs using Eqs. (4) and (5), one has to integrate over the electronic coordinates. This is achieved numerically using the MOLPRO derivative couplings (DDR) procedure for  $A(R)$ , and by using central finite difference scheme for

the derivative to obtain  $B(R)$ . The spectroscopical description of the target, including the 15 vibrational levels of the ground state of  $\text{NeH}^+$  were obtained by using the Numerov-Cooley method [26, 27] to solve the nuclear-motion Schrödinger equation.

### III. RESULTS AND DISCUSSIONS

Figure 1 displays the *ab initio* PECs of the ground electronic state of  $\text{NeH}^+$  ( $^1\Sigma^+$ ) (blue curve), the repulsive ground electronic state of NeH, and the mono-excited Rydberg states of NeH for both symmetries  $^2\Sigma^+$  and  $^2\Pi$ , up to the  $\text{Ne}+\text{H}(n=3)$  dissociation limit. The dissociative ground state of the neutral  $\text{X } ^2\Sigma^+$  correlates to the  $\text{Ne}+\text{H}(1s)$  atomic limit, where Ne stands for the  $^1S_0$  ground state of atomic neon. The excited states correlating with the  $\text{Ne}+\text{H}(n=2)$  limits from bottom to top are  $\text{A } ^2\Sigma^+$  -  $\text{B } ^2\Pi$  -  $\text{C } ^2\Sigma^+$ , and the states tending to the  $\text{Ne}+\text{H}(n=3)$  are  $4 ^2\Sigma^+$  -  $2 ^2\Pi$  -  $5 ^2\Sigma^+$ . Our results - black curves in Fig. 1 - compare well with those from Theodorakopoulos et al.[20] - red curves.

Figure 2 shows the NACs  $A(R)$  corresponding to Eq. (4) between the molecular states having  $^2\Sigma^+$  (solid curves) and  $^2\Pi$  (dashed curves) symmetry, up to the  $\text{Ne}+\text{H}(n=3)$  dissociation limit. The couplings involving the highest excited state  $5 ^2\Sigma^+$  are not shown as their magnitudes are negligible (approximately  $10^{-8} a_0^{-1}$ ). One can notice that the couplings of the  $^2\Sigma^+$  states are the more important ones, while the coupling involving the two  $^2\Pi$  states is about one order of magnitude smaller. Similarly to PECs, we have compared our NACs (in black) with those calculated by Theodorakopoulos et al [20] presented in red. One can conclude that the current results are consistent with the previous ones. The sharp peak of the A-C coupling is due to the strong interaction between these two electronic states.

Figure 3 contains all the NACs  $A(R)$  given by Eq. (4) (already shown in Fig. 2), in comparison with  $B(R)$  given by Eq. (5). One can see that the most significant  $B(R)$  NAC is the A-C one, followed by C-4, X-A, X-C, X-4, A-4, B-2, which predicts the importance of the Rydbergs correlating with the  $\text{Ne}+\text{H}(n=3)$  limit for the inter-nuclear dynamics.

In order to fully characterize the molecular system, we have calculated the major spectroscopic data of the molecular target and for the neutral system. They are shown in tables II, III, IV and V, where our results are compared with previous theoretical results [3, 4, 22, 23, 30-38], experimental results [28, 29, 33], and data from the NIST chemistry webbook [39].

Table II refers to the molecular ion, and shows values for its equilibrium geometry, the potential energy at equilibrium, and its dissociation energy. We compare our calculated parameters with other theoretical results [3, 4, 22, 23, 30-38], and evaluate relative differences of the dissociation energy in contrast to the experimental measurements [28, 29]. Our results agree well with existing experimental and other theoretical results, typically within 2%, except for a few studies [3, 23, 31, 36, 37] which employed lower levels of theory.

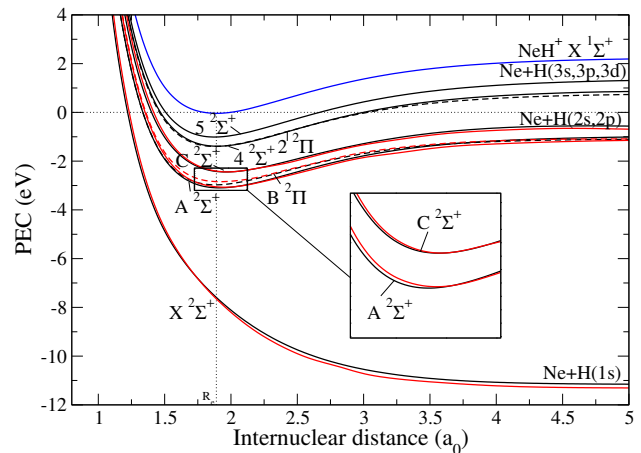


FIG. 1: *Ab initio* PECs of the ground electronic state of  $\text{NeH}^+$  and of the lowest - ground and Rydberg - electronic states of NeH. Black solid lines stand for the neutral with  $^2\Sigma^+$  symmetry, black dashed lines for the neutral with  $^2\Pi$  symmetry, and the solid blue line corresponds to the ion's ground state  $\text{X } ^1\Sigma^+$ . Our results are compared with the calculations of Theodorakopoulos et al.[20] (red lines).

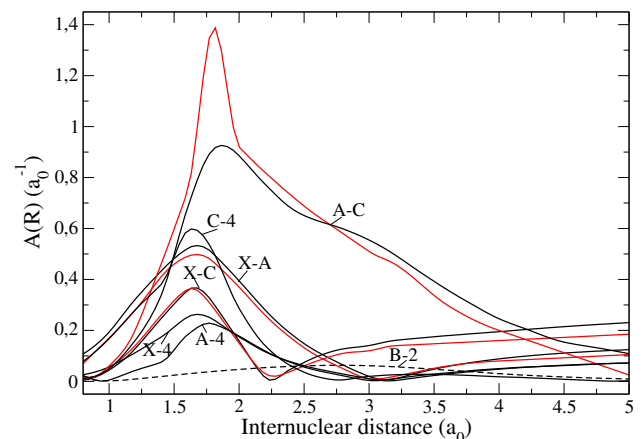


FIG. 2: Radial non-adiabatic couplings  $A(R)$ . The color code is the same as for Fig. 1.

In table III, we list all the 15 vibrational levels of the cation calculated using the Numerov-Cooley method and compare them with experimental observations [28, 33]. The relative differences obtained are below 1%, which confirms the accuracy of our structure calculations.

Table IV gives the dissociation limits of the electronic states of  $\text{NeH}^+$  ( $\text{X } ^1\Sigma^+$ ) and of the NeH Rydberg states relative to  $\text{Ne}+\text{H}(n=1)$ , in comparison with previously computed limits [22, 23] and with data from the NIST chemistry webbook [39].

Finally, table V contains the excitation energies of  $\text{NeH}^+$  and of NeH electronic states relative to the  $\text{A } ^2\Sigma^+$  state of NeH for all electronic states above the same  $\text{A } ^2\Sigma^+$  state, calculated at the equilibrium distance of the ion.

The corresponding energy differences  $\Delta E(R_e)$  are compared with the previous calculations [22, 23]. One may

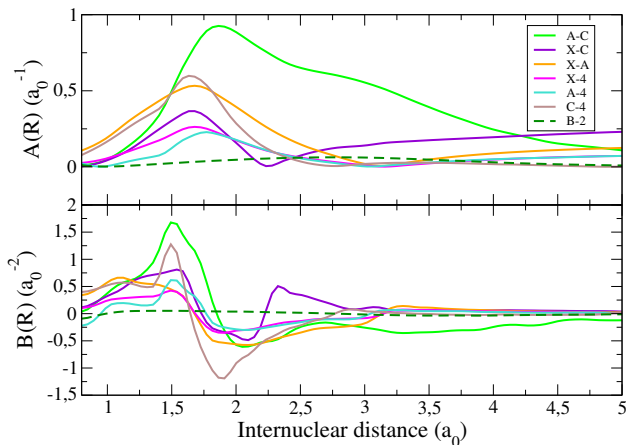


FIG. 3: First-derivative radial non-adiabatic couplings  $A(R)$  and second-derivative radial non-adiabatic couplings  $B(R)$ , between the states of NeH.

TABLE II: Equilibrium separation ( $R_e$ ), absolute minimum energy ( $E(R_e)$ ) and well-depth ( $D_e$ ) for  $\text{NeH}^+$  ( $X^1\Sigma^+$ ) PECs: comparison with theoretical as well as experimental data from the literature.  $\epsilon_0$  represents percentage difference between the calculations and the experimental measurements for  $D_e$ .

Source	Level of theory	Basis set	$R_e$ ( $a_0$ )	$E(R_e)$ (Hartree)	$D_e$ (eV)	$\epsilon_0$ (%)
Exp [28, 29]			1.8731	-	2.275	
Present	MRCI <sup>a</sup>	sec. II	1.8920	-128.8965	2.269	0.3
Theory [30]	CCSD(T)	CBS	1.8733	-128.9536	2.292	0.7
Theory [30]	MRCI+Q	AV6Z	1.8733	-128.9485	2.296	0.9
Theory [31]	-	-	1.8729	-	2.179	4.4
Theory [32]	MRCI	aug-AO	1.8756	-	2.288	0.5
Theory [4]	CI	TZP	1.8935	-	2.320	1.9
Theory [23]	SCF	cc-pVTZ	1.8627	-128.881	2.370	4.0
Theory [3]	CI	aug-AO	1.8708	-	2.148	5.9
Theory [33]	MRCISD <sup>b</sup>	-	1.8731	-	2.296	0.9
Theory [22]	MRDCI	aug-AO	1.8948	-128.9787	2.290	0.7
Theory [34]	MRCI <sup>b</sup>	aug-AO	1.8765	-	2.310	1.5
Theory [35]	CEPA <sup>c</sup>	AO	1.8820	-128.3490	2.276	0.1
Theory [36]	SCF	STO	1.850	-128.6242	2.10	8.3
Theory [36]	CI	STO	1.8689	-128.6818	2.270	0.2
Theory [37]	MRDCI	aug-AO	1.8670	-	2.430	6.4
Theory [38]	MRCI	cc-pV5Z	1.8730	-	2.299	1.0

<sup>a</sup> Atomic orbitals calculated with MCSCF.

<sup>b</sup> Atomic orbitals calculated with SCF-CASSCF.

<sup>c</sup> Atomic orbitals calculated with SCEP.

All other: Atomic orbitals calculated with SCF.

notice that, except for the B state, where a significant gap occurs, the agreement is satisfactory.

Our computational framework does not take into account the Rydberg states of NeH built on the excited states of the  $\text{NeH}^+$  ion. For several molecular species, these 'intruder' states play a visible role in the spectroscopy of the neutral and in its dynamics. However, this happens only when the lowest excited states of the ion are close to the ground one, which is not the case for  $\text{NeH}^+$  [32]. Therefore, we believe that our results

TABLE III: Calculated vibrational energy levels  $E_{v_i^+}$  (eV) for  $\text{NeH}^+$  ( $X^1\Sigma^+$ ) with respect to  $E_0 = -128.88998$  Hartree, and comparison with experimental values from [28, 33]. The relative differences between our results and the experimental data are given by  $\epsilon_0$ (%).

$v_i^+$	This work	Exp	$\epsilon_0$ (%)
1	0.33524	0.33197	0.98
2	0.64055	0.63593	0.72
3	0.91920	0.91267	0.71
4	1.16981	1.16138	0.72
5	1.39213	1.38233	0.70
6	1.58560	1.57472	0.69
7	1.74969	1.73799	0.67
8	1.88330	1.87132	0.64
9	1.98643	1.97391	0.63
10	2.05881	2.04629	0.61
11	2.10262	2.08983	0.61
12	2.12384	2.11051	0.63
13	2.12384	2.11731	0.31
14	2.12384	2.11895	0.23

TABLE IV: Comparison of our computed  $\text{NeH}^+$  ( $X^1\Sigma^+$ ) and NeH Rydberg states dissociation limits relatively to  $\text{Ne}+\text{H}(n=1)$  (eV) with previous theoretical results [22, 23] and data from NIST chemistry webbook [39]. The relative differences between our results and the NIST data are given by  $\epsilon_0$ (%).

level	This work	[22]	[23]	NIST	$\epsilon_0$ (%)
$n=2$	10.20509	10.21788	10.20209	10.19880	0.062
$n=3$	12.09383	12.10853	12.09201	12.08750	0.052
H IP	13.55481	13.56815	13.57945	13.59840	0.322

are accurate, since not being affected by the core-excited Rydberg states effects.

#### IV. CONCLUSIONS

The potential energy curves for the ground state  $^1\Sigma^+$  of  $\text{NeH}^+$  ion and for the lowest five  $^2\Sigma^+$  states and two  $^2\Pi$  states of NeH molecule have been computed with high precision using the MOLPRO quantum chemistry suite at the MCSCF-MRCI level of theory, employing an extended complete active space (CAS) and augmented basis sets optimized for dissociation up to  $\text{Ne}+\text{H}(n=3)$ . The results show good agreement with previous experimental and theoretical studies, particularly with the work of Theodorakopoulos et al. [20], Petsalakis et al. [22], and Lo et al. [23] for some of these states. While the non-adiabatic couplings  $A(R)$  between the states (A-C, X-A, X-C) up to  $\text{Ne}+\text{H}(n=2)$  had already been addressed by Theodorakopoulos et al. [20], our calculations went beyond this producing further, namely both the couplings  $A(R)$  and  $B(R)$  between states dissociating up to the limit  $\text{Ne}+\text{H}(n=3)$  - X-4, A-4, C-4, X-5, A-5, C-5 for the  $^2\Sigma^+$  symmetry, and B-2 for the  $^2\Pi$  symmetry. These couplings are essential for the calculation of cross sections and rate coefficients in low-energy collisions between electrons and  $\text{NeH}^+$  [40, 41]. Work on this is currently in

TABLE V: Energy differences  $\Delta E(R_e)$  (eV) at the equilibrium distance  $R_e$  of the  $\text{NeH}^+$  ground electronic state, between several states and the  $\text{NeH}$  lowest excited electronic state ( $A \ ^2\Sigma^+$ ). The results are compared with the previous theoretically obtained data [22, 23].

State	This work	[22]	[23]
B $^2\Pi$	0.12045	0.22365	0.17499
C $^2\Sigma^+$	0.67190	0.70451	0.64747
2 $^2\Pi$	1.69663	1.63268	1.66243
4 $^2\Sigma^+$	1.70531	1.72214	1.62743
5 $^2\Sigma^+$	2.08265	1.99053	-
X $^1\Sigma^+$	3.05459	3.14235	3.07987

progress.

### Data availability

The data underlying this article will be shared on reasonable request to the corresponding author.

### Acknowledgments

The authors acknowledge support provided by the Fédération de Recherche Fusion par Confinement Magnétique (CNRS and CEA), La Région Normandie, LabEx EMC3 through projects PTOLEMEE, COMUE Normandie Université and the Institute for Energy, Propulsion and Environment (FR-IEPE). J.Zs.M. is grateful for financial support from the National Research, Development and Innovation Fund of Hungary, under the FK 19 funding schemes with project number FK 132989. This work was granted access to the HPC/AI resources of [CINES/IDRIS/TGCC] under the allocation 2023-2024 [AD010805116R2] made by GENCI.

- 
- [1] D. Zajfman, B. A. Mitchell, James, B. R. Rowe, and D. Schwalm. *Dissociative Recombination, Theory, Experiment And Applications III*. World Scientific, 1996.
- [2] J. B. A. Mitchell. Atomic and Plasma-Material Interaction for Fusion. *Vienna: IAEA*, page 97, 2001.
- [3] J. B. A. Mitchell, O. Novotny, G. Angelova, J. L. LeGarrec, C. Rebrion-Rowe, A. Svendsen, L. H. Andersen, A. I. Florescu-Mitchell, and A. E. Orel. *J. Phys. B: At. Mol. Phys.*, 38:693, 2005.
- [4] V. Ngassam, A. I. Florescu-Mitchell, and A. E. Orel. *Phys. Rev. A*, 77:042706, 2008.
- [5] R. Güsten, H. Wiesemeyer, D. Neufeld, K. M. Menten, U. U. Graf, K. Jacobs, B. Klein, O. Ricken, C. Risacher, and J. Stutzki. *Nature*, 568:357, 2019.
- [6] B. K. Sarpal, J. Tennyson, and L. A. Morgan. Dissociative recombination without curve crossing: study of  $\text{HeH}^+$ . *J. Phys. B: At. Mol. Opt. Phys.*, 27:5943–5953, 1994.
- [7] S. L. Guberman. *Phys. Rev. A*, 49:R4277, 1994.
- [8] O. Novotný, P. Wilhelm, D. Paul, A. Kalosi, S. Saurabh, A. Becker, K. Blaum, S. George, J. Göck, M. Grieser, et al. *Science*, 365:676, 2019.
- [9] R. Čurík, D. Hvizdoš, and C. H. Greene. *Phys. Rev. Lett.*, 124:043401, 2020.
- [10] D. Hvizdoš, C. H. Greene, and R. Čurík. *Phys. Rev. A*, 101:012709, 2020.
- [11] M. J. Barlow, B. M. Swinyard, P. J. Owen, J. Cernicharo, H. L. Gomez, R. J. Ivison, O. Krause, T. L. Lim, M. Matsumura, S. Miller, et al. *Science*, 342:1343, 2013.
- [12] J. B. A. Mitchell, O. Novotny, J. L. LeGarrec, A. Florescu-Mitchell, C. Rebrion-Rowe, A. V. Stoloyarov, M. S. Child, A. Svendsen, M. A. El Ghazaly, and L. H. Andersen. *J. Phys. B: At. Mol. Phys.*, 38:L175, 2005.
- [13] A. Abdoulanziz, F. Collboc, D. A. Little, Y. Moulane, J. Zs. Mezei, E. Roueff, J. Tennyson, I. F. Schneider, and V. Laporta. *MNRAS*, 479:2415, 2018.
- [14] E. Djuissi, A. Bultel, J. Tennyson, I. F. Schneider, and V. Laporta. *PSST*, 31:114012, 2022.
- [15] Á. Kálosi, M. Grieser, L. W. Isberner, H. Kreckel, Å. Larson, D. A. Neufeld, A. E. Orel, D. Paul, D. W. Savin, S. Schippers, et al. *Phys. Rev. A*, 110:022816, 2024.
- [16] M. Sil, A. Das, R. Das, R. Pandey, A. Faure, H. Wiesemeyer, P. Hily-Blant, F. Lique, and P. Caselli. Fate and detectability of rare gas hydride ions in nova ejecta. *Astron. Astrophys.*, 692:A264, 2024.
- [17] R. A. Theis, W. J. Morgan, and R. C. Fortenberry. *MNRAS*, 446(1):195, 2015.
- [18] G. J. Schwarz. *ApJ*, 577(2):940, 2002.
- [19] G. Theodorakopoulos, S.C. Farantos, R.J. Buenker, and S.D. Peyerimhoff. *J. Phys. B: At. Mol. Phys.*, 17:1453, 1984.
- [20] G. Theodorakopoulos, R. J. Buenker, and I. D. Petsalakis. *J. Phys. B: At. Mol. Phys.*, 20:5335, 1987.
- [21] S. Baer, D. G. Fleming, J. J. Sloan, D. J. Arseneau, M. Kolbuszewski, J. Wright, M. Senba, J. J. Pan, and R. Snooks. *J. Chem. Phys.*, 101:1202, 1994.
- [22] I. D. Petsalakis, G. Theodorakopoulos, Y. Li, G. Hirsch, R. J. Buenker, and M. S. Child. *J. Chem. Phys.*, 108:7607, 1998.
- [23] J. M. H. Lo, M. Klobukowski, D. Bielińska-Waż, G. H. F. Diercksen, and E. W. S. Schreiner. *J. Phys. B: At. Mol. Phys.*, 38:1143, 2005.
- [24] H. J. Werner, P. J. Knowles, G. Knizia, F. R. Manby, M. Schütz, P. Celani, W. Györfy, D. Kats, T. Korona, R. Lindh, et al. Molpro, version 2022.1, a package of ab initio programs, 2022.
- [25] R. P. Brady, C. Drury, S. N. Yurchenko, and J. Tennyson. *J. Chem. Theory Comput.*, 20:2127, 2024.
- [26] B. V. Noumerov. *Mon. Not. Roy. Astron. Soc.*, 84:592, 1924.
- [27] B. Numerov. *Astron. Nachr.*, 230:359, 1927.
- [28] R. S. Ram, P. F. Bernath, and J. W. Brault. *J. Mol. Spectrosc.*, 113:451, 1985.
- [29] H. Hotop, T. E. Roth, M. W. Ruf, and A. J. Yencha. *Theor. Chem. Acc.*, 100:36, 1998.
- [30] M. J. Montes de Oca-Estevéz and R. Prosmiti. *Front.*

- Chem.*, 9:664693, 2021.
- [31] J. A. Coxon and P. G. Hajigeorgiou. *J. Mol. Spectrosc.*, 330:63, 2016.
- [32] B. Gerivani, A. Shayesteh, and A. Maghari. *Comput. Theor. Chem.*, 1070:82, 2015.
- [33] S. Civiš, J. Šebera, V. Špirko, J. Fišer, W. P. Kraemer, and K. Kawaguchi. *J. Mol. Struct.*, 695:5, 2004.
- [34] W. P. Kraemer, M. Juřek, and V. Špirko. In D Papoušek, editor, *Vibration-Rotational Spectroscopy And Molecular Dynamics: Advances in Quantum Chemical and Spectroscopical Studies of Molecular Structures and Dynamics*, page 516. WORLD SCIENTIFIC, 1997.
- [35] P. Rosmus and E. A. Reinsch. *Z. Naturforsch. A*, 35, 1980.
- [36] V. Bondybey, P. K. Pearson, III. Schaefer, and F. Henry. *J. Chem. Phys.*, 57:1123, 1972.
- [37] Y. Wan, P. Leiberman, R. Buenker, S. D. Loch, D. R. Schultz, and P. C. Stancil. *ApJ*, 881:3, 2019.
- [38] P. G. Yan and J. F Babb. *ApJ*, 961:43, 2024.
- [39] P. Linstorm. Nist chemistry webbook, nist standard reference database number 69. *J. Phys. Chem. Ref. Data, Monograph*, 9:1, 1998.
- [40] A. Giusti. *J. Phys. B: At. Mol. Phys*, 13:3867, 1980.
- [41] J. Zs. Mezei, K. Chakrabarti, M. D. Epée Epée, O. Motapon, C. H. Yuen, M. A. Ayouz, N. Douguet, S. Fonseca dos Santos, V. Kokoouline, and I. F. Schneider. *ACS Earth Space Chem.*, 3:2376, 2019.